UC Berkeley
UC Berkeley Previously Published Works

Title

Electron microscopy evidence of gadolinium toxicity being mediated through cytoplasmic membrane dysregulation

Permalink

Journal

ISSN

Authors

Arino, Trevor
Faulkner, David
Bustillo, Karen C
et al.

Publication Date

DOI

Copyright Information

Peer reviewed

Electron microscopy evidence of gadolinium toxicity being mediated through cytoplasmic membrane dysregulation

Trevor Arino [ID][1,2,‡], David Faulkner [ID][1,§,‡], Karen C. Bustillo [ID][3], Dahlia D. An [ID][1], Danielle Jorgens [ID][4], Solène Hébert[1], Carla McKinley [ID][1,2], Michael Proctor[5], Alex Loguinov [ID][5], Christopher Vulpe [ID][5] and Rebecca J. Abergel [ID][1,2,*]

[1]Chemical Sciences Division, Lawrence Berkeley National Laboratory, Berkeley, CA 97420, USA, [2]Department of Nuclear Engineering, University of California Berkeley, Berkeley, CA 94720, USA, [3]National Center for Electron Microscopy, Molecular Foundry, Lawrence Berkeley National Laboratory, Berkeley, CA 94720, USA, [4]Electron Microscope Laboratory, University of California Berkeley, Berkeley, CA 94720, USA and [5]Center for Environmental and Human Toxicology, Department of Physiological Sciences, College of Veterinary Medicine, University of Florida, Gainesville, FL 32611, USA
***Correspondence:** Chemical Sciences Division, Lawrence Berkeley National Laboratory, Berkeley CA 94720, USA. E-mail: rjabergel@lbl.gov
‡These authors contributed equally to this work.
§Present address: California Department of Toxic Substances Control, Berkeley Regional Office, 700 Heinz Avenue, Suite 200, Berkeley, CA 94710, USA.

Abstract

Past functional toxicogenomic studies have indicated that genes relevant to membrane lipid synthesis are important for tolerance to the lanthanides. Moreover, previously reported imaging of patient's brains following administration of gadolinium-based contrast agents shows gadolinium lining the vessels of the brain. Taken together, these findings suggest the disruption of cytoplasmic membrane integrity as a mechanism by which lanthanides induce cytotoxicity. In the presented work we used scanning transmission electron microscopy and spatially resolved elemental spectroscopy to image the morphology and composition of gadolinium, europium, and samarium precipitates that formed on the outside of yeast cell membranes. In no sample did we find that the lanthanide contaminant had crossed the cell membrane, even in experiments using yeast mutants with disrupted genes for sphingolipid synthesis—the primary lipids found in yeast cytoplasmic membranes. Rather, we have evidence that lanthanides are co-located with phosphorus outside the yeast cells. These results lead us to hypothesize that the lanthanides scavenge or otherwise form complexes with phosphorus from the sphingophospholipid head groups in the cellular membrane, thereby compromising the structure or function of the membrane, and gaining the ability to disrupt membrane function without entering the cell.

Graphical abstract
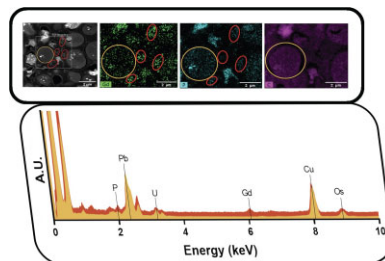
High-resolution electron microscope images and corresponding elemental maps showing substantial evidence of extracellular toxicity of lanthanides to exposed yeast cells.

Introduction

Lanthanide metals have many applications across a variety of industries, from small-scale electronics to medical imaging, and they play an important role in the technologies that facilitate modern life. However, since lanthanides are nearly always found as geochemical alloys and minerals, there is little historical precedent for exposure to these metals individually, and pure lanthanide compounds are a novelty of the last half century.[1] Consequently, relatively little is known about chronic effects that might result from exposure to these "rare earth" elements, in part due to their rarity as pure ores and in part due to historical assumptions of their safety.[2]

In 2006, the first of many papers were published that identified some types of gadolinium-based contrast agents (GBCAs) as causative agents of nephrogenic systemic fibrosis (NSF) in patients who underwent magnetic resonance imaging, a pathology that has been virtually eliminated as patients at risk of kidney failure no longer receive GBCAs. However, patients not at risk for kidney failure continue to receive GBCAs and evidence began to emerge suggesting that these contrast agents also accumulate in the brain and skin.[3–7] Due to the accumulation of gadolinium in organs including, but not limited to the kidneys, this work adopts the term "symptoms associated with gadolinium exposure (SAGE)," originally proposed by McDonald *et al.* instead of the more exclusive term, NSF.[8] Examples of gadolinium inclusions found in tissues collected from patients experiencing SAGE symptoms have been commonly found as insoluble gadolinium phosphates co-localized with other divalent metals.[7,9,10] Follow-up studies demonstrated that gadolinium deposits formed along blood vessels in the brain, most significantly in the dentate nucleus, but no indication of histopathological change was observed that could be attributed to the gadolinium.[11] Much of the evidence suggested that gadolinium need not enter cells to produce deleterious effects: several groups have shown that gadolinium (like other lanthanides) can disrupt voltage-gated ion channels, and generally interact with membrane proteins.[12–15] Cheng *et al.* demonstrated that gadolinium can induce pore formation on the surface of mouse erythrocytes, and that this effect is reversed through the addition of the chelating agent EDTA.[16] It is worth noting that lanthanides have been shown to aggregate as $LnPO_4$ and to readily induce intracellular toxicity in some methylotrophic microbial organisms, even though the structure and function of such prokaryotic cells are quite different from mammalian cells.[17–20] Other studies show that lanthanide cations improved transformation of plasmids in *Escherichia coli* in lower concentrations than are required for calcium shock.[21] Terbium, as Tb^{3+}, has been shown to increase uptake of cisplatin in human ovarian cancer cell lines, and lanthanum, as La^{3+}, stimulates Ca^{2+} uptake in hepatocytes and thymocytes.[22,23] Given this evidence, it is reasonable to suspect that lanthanides may induce a wide range of cell responses.

In a previous publication, we described several toxicological mechanisms suggested by gene ontology analysis of yeast functional toxicogenomic data, including two—disruption of lipid homeostasis and membrane transport systems—that have been identified by other groups performing similar "omics-level" analyses.[24] Our toxicogenomic data and data from other studies suggested that we should observe deposits of lanthanides in many intracellular compartments within exposed yeast cells; however, the present investigation with transmission electron microscopy (TEM) did not reveal lanthanide ions inside the cell, even though yeast growth was significantly inhibited by lanthanide exposure. Instead, we observed nanoprecipitate formation outside the cells with a consistent morphology and co-location with phosphorus. Both energy dispersive spectroscopy (EDS) and inductively coupled plasma optical emission spectroscopy (ICP-OES) techniques validated that these deposits were composed of lanthanides. Curiously, these findings remained unchanged when we exposed mutant strains with known defects in phospholipid synthesis such as *csh1, csg2,* and *sur1*.[25,26] Although the mutant strains demonstrated more significant growth inhibition upon lanthanide exposure than the corresponding wildtype (WT), none of the mutant strains showed accumulation of lanthanides in any intracellular compartment. The *sso2* membrane transport protein mutant was used as a control in EDS experiments, with similar results. Finally, we treated the yeast mutants with both lanthanides and calcium

to see if we could rescue the growth inhibition effect and observed significant increases in yeast growth upon the addition of calcium. This result was particularly surprising, given that *csh1, csg2,* and *sur1* are known to be highly sensitive to calcium, and suggests a mechanism by which calcium rescues the phenotype.

Our study provides additional evidence that global phospholipid regulation is disrupted by lanthanide scavenging phosphorus from the cell surface, suggesting that patients with lipid synthesis or storage disorders may be at greater risk of lanthanide toxicity. Further, calcium appears to restore normal cell growth in yeast exposed to lanthanides, hinting at a possible strategy for reducing or reversing lanthanide toxicity.

Methods
Yeast culture (*Saccharomyces cerevisiae*)
The *csh1, csg2, sso2,* and *sur1* mutants used in this study are derived from the BY4743 lineage leu2D0/leu2D0 MATa/ahis3D1/his3D1 met15D0/MET15lys2D0/LYS2, as described by Winzeler *et al.*, which was also used in our previous functional toxicogenomic reports.[27,28] Therefore, BY4743 served as our WT (control) strain. Both WT and mutant strains were purchased from the American Type Culture Collection (ATCC) as glycerol stocks stored at −80°C.[29] Strains were grown by streaking samples from glycerol stocks onto yeast extract-peptone-dextrose (YPD) agar using the four-quadrant method. Plates were incubated at 30°C for 1–2 days. YPD liquid media was prepared using 1% Bacto™ Yeast Extract Technical, 2% Bacto™ Peptone and 2% Dextrose solution autoclaved at 121°C for 30 min. Plates of solid YPD media for yeast growth were prepared using the same recipe with the addition of 2% Bacto™ Agar.

Dose–response curves generation
Single colonies were picked using a single-use sterile loop and incubated in YPD in a 15 ml Falcon tube overnight in an incubator-shaker at 30°C and 200 rpm. Upon reaching the log phase, these yeast strains were diluted to 0.0165 optical density at 600 nm (OD600) in fresh YPD and added to clear 96-well plates (Grenier Bio-One, Monroe, NC, USA) as 100 μl aliquots per well. Cultures were treated with either aqueous lanthanides (Ln=La, Pr, Nd, Sm, Eu, Dg, Tb, Dy, Ho, Er, Tm, Yb, and Lu) in the form of $LnCl_3$, both $LnCl_3$ and $CaCl_2$, or with 1% HCl as the vehicle control. Lanthanide concentrations ranged from 0.05 mmol to 0.20 mmol, depending on the IC_{20} values calculated in previous publications.[24] To exhibit calcium effects, the concentration of culture solutions was brought to 100 mmol of Ca^{2+}, using $CaCl_2$. Well plates were incubated at 30°C with continuous 200 rpm shaking inside a Tecan Genios microplate reader (Tecan Group Ltd, Männendorf, Switzerland). OD600 of each well was measured every 15 min for a period of 24 h.

Cell preparation for ICP-OES
After yeast had been exposed to lanthanides for 12 h, samples were centrifuged at 6000 rpm for 6 min and the media was aspirated, leaving a pellet. The pellet was resuspended in 200 μl of calcium-free, magnesium-free Dulbecco's Phosphate-Buffered Saline (DPBS) and transferred to a microcentrifuge tube. The microcentrifuge tubes were centrifuged at 8000 rpm for 6 min, then the media was aspirated as before, and the pellet was resuspended in 200 μl calcium-free, magnesium-free DPBS. This wash step was repeated twice so that the pellet was washed at least three times. After the pellets had been washed

three times, they were resuspended in 150 μl DPBS and 50 μl of the resulting suspension was transferred to a fresh 15 ml Falcon tube containing 100 μl 6N HNO_3, 100 μl 37% HCl, and 4750 μl Milli-Q water for digestion. Digestion tubes were incubated for 12 h at 70°C with 200 rpm shaking. OD measurements were taken from the remaining yeast DPBS solutions. A multi-element ICP-OES standard was prepared in 2% HNO_3.

Electron microscopy sample preparation

Single colonies were picked using a single-use sterile loop and incubated in 3 ml YPD overnight in an incubator-shaker at 30°C and 200 rpm. Upon reaching log phase, these yeast strains were diluted to 0.0165 OD600 in fresh YPD. Cultures were treated with either aqueous lanthanides in the form of $LnCl_3$ and brought to a final concentration of 0.16 mmol, or with an equal concentration of HCl as the vehicle control. The cultures were returned to the incubator-shaker for 12 h at 30°C and 200 rpm.

High pressure freezing with freeze substitution: Yeast cells were concentrated via vacuum filtration onto 0.45 μm neolone nylon membranes (MilliporeSigma, Burlington, MA, USA). The concentrated cell paste was scraped off the membrane with a toothpick and deposited into 2 mm wide by 50 μm or 100 μm deep aluminum freezing hats. The cells were then cryo-immobilized using a BAL-TEC HPM-010 high-pressure freezer (BAL-TEC, Inc., Carlsbad, CA, USA). The samples were placed in freeze-substitution medium made up of 1% osmium tetroxide, 0.1% uranyl acetate, and 5% double-distilled water in acetone. All samples were freeze-substituted following the Quick Freeze Substitution method outlined by McDonald and Webb.[30] Following freeze-substitution, the samples were rinsed in pure acetone and then samples were progressively infiltrated while rocking with Epon resin (EMS, Hatfield, PA, USA).

Scanning TEM (STEM) sample preparation: Cells were fixed in a solution of 3% glutaraldehyde (EMS, Hatfield, PA, USA) in 1× phosphate buffered saline (PBS), pH 7.4, for at least 1 h prior to being stabilized in 1% low melting point agarose (EMS #10207). Agarose was diced into 0.5 mm cubes, then fixed overnight. Samples were rinsed (3×; 10 min, RT) in 1× PBS, pH 7.4, and then immersed in a solution of 1% osmium tetroxide with 1.6% potassium ferrocyanide in 1× PBS for 1 h. Samples were rinsed (3×; 10 min, RT) in a solution of 1× PBS; then subjected to an ascending acetone gradient (10 min; 35%, 50%, 70%, 80%, 90%, 100%) followed by pure acetone (3×; 10 min, RT). Samples were progressively infiltrated while rocking with Epon resins (EMS, Hatfield, PA, USA) and polymerized at 60°C for 24–48 h.

Thin sections of (90 nm) of Epon blocks were cut using a Leica UC6 (Leica Wetzlar, Germany) and collected onto formvar-coated copper 50 mesh grids or copper slot grids. When needed, grids were post-stained with 2% aqueous uranyl acetate followed by Reynold's lead citrate, for 5 min each.

STEM and energy dispersive spectroscopy

Investigations of morphology were conducted on an FEI TitanX 60-300 microscope at the National Center for Electron Microscopy of the Lawrence Berkeley National Laboratory (LBNL), operated at 200 kV. Most scanning images were acquired in high-angle annular dark field (HAADF) mode such that brightness of the feature increases with the atomic number of the element. The FEI TitanX was also equipped with a Bruker SuperX EDS detector, which was used to collect all EDS data as a function of scan position resulting in elemental maps from the X-ray edges.

Results and discussion

We anticipated that TEM would show examples of the characteristic filamentous or globular lanthanide deposits observed in previous publications.[20] Primarily, we expected to find lanthanides in the vacuole, Golgi, or endosomal compartments, since *S. cerevisiae* regulates intracellular ion content in response to environmental conditions using these organelles for ion storage and release.[31] However, in all WT samples exposed to lanthanides (Ln=Sm, Eu, and Gd) precipitate formation was observed outside the cells, not inside (Fig. 1). Figure 1 shows a HAADF-STEM image of a WT yeast sample that has been treated with $GdCl_3$. The brightest features in Fig. 1A arise from the heavy element staining (U, Os, and Pb) as well as from the presence of Gadolinium. The white box in 1A shows the region from which the EDS spectrum image was acquired with 1B through 1D showing the Gd_L, P_K, and C_K elemental maps. However, an EDS map is constructed by adding color to a pixel that generated an X-ray from a band of energies centered around the X-ray edge, whether that X-ray is from the bremsstrahlung background or decay from a previous edge or whether it is truly generated from the element. We also note that regions of heavy element scattering will generate more background signal than regions of less scattering. The spectra in Fig. 1E show how one can distinguish the two. The gold trace is from a region of the sample that does not contain the precipitates as shown by the gold ellipse; the green pixels inside the gold ellipse are from the background. The red trace is a sum of the regions defined by the red ellipses where the lanthanide precipitates reside; the Gd signal is clearly shown above the background, indicating that the green pixels in the Gd_L map are truly from the element. Based on the acquired data, we are able to measure Gd at 0.01 atomic % in the TEM samples.

Analysis of the whole yeast cell shows no Gd penetration into the cell. The Gd_{L_3} edge is visible at 6.056 keV and is expressed in the precipitates (circled in red) but not in the cell area, represented in gold in Fig. 1E. Pb, U, Os are also labeled on the EDS spectrum, as these metals were incorporated into the cells during the fixation process as staining agents and to make the cells more robust to the high beam currents necessary to generate EDS data.[32,33] Cu appears on the EDS spectrum because of the TEM grids and TEM holder hardware, but was not intentionally introduced to any samples. Gd and P can be seen to co-localize, and quantification of the areas under the respective peaks produces a nearly 1:1 ratio of the two elements. Based on precedent established in previous studies, the species formed is likely $GdPO_4$ and confirmed by subsequent control experiments and thermodynamic data reported below.[6,7]

The morphology of the precipitates, as imaged using HAADF-STEM, was consistent and unique, as displayed throughout increasing magnification in Fig. 2A–D. Figure 2D shows that the precipitates are constructed of small seed-like components, 1–2 nm in diameter, which cluster together in a loose morphology, often in a ring-like pattern with a less-dense center. This morphology was consistent across all tested lanthanides and all mutations. The distinct morphology made it easy to identify the location of lanthanides in support of the EDS data. Regions of the cell that were stained with U, Os, or Pb also exhibited bright contrast, but these regions did not exhibit such distinct morphology. The consistent morphology also made it possible to screen large areas to evaluate the location of the precipitates, which were found close to the cell surface though not within it. Instead, we observed the precipitates localized next to the membranes, embedded in the epoxy resin used in the microtome sample preparation process.
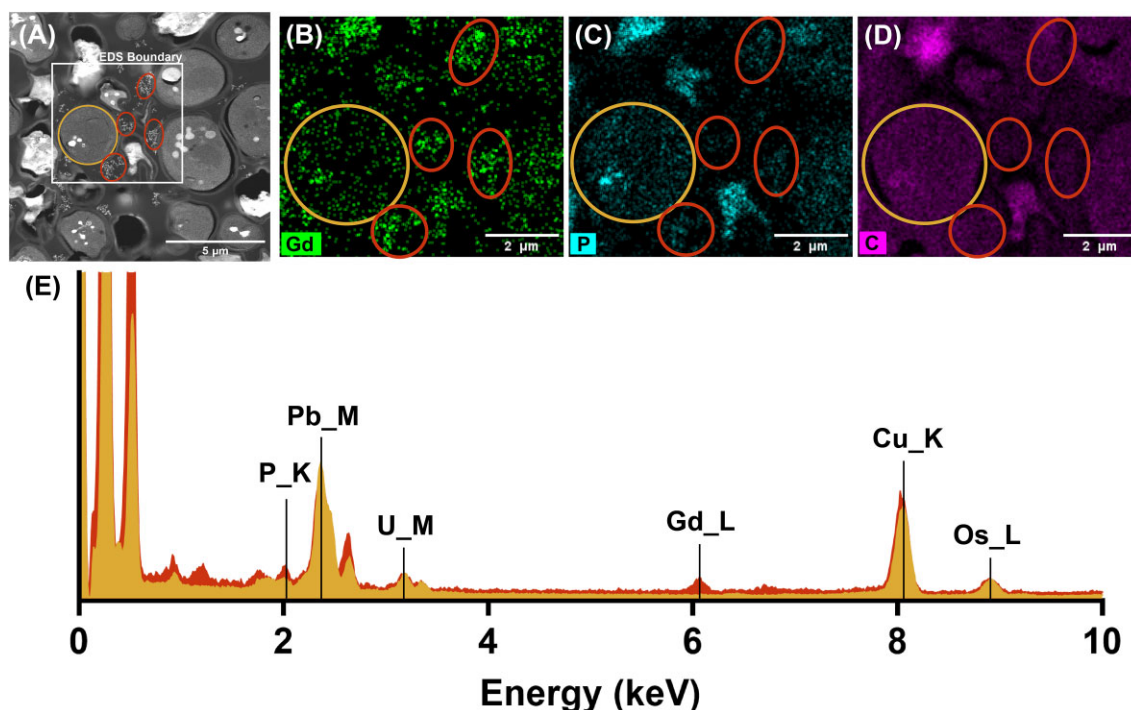
Fig. 1 (A) STEM image of wild type yeast strain (BY4743) treated with Gadolinium. Gd precipitates in amorphous nanoclusters outside of the cell. Images (B)–(D) are EDS maps of elements present in image (A). (B) Gd nanoprecipitates localized outside of the cell. (C) Co-localization of phosphorous and Gd outside of cell. (D) Carbon EDS map. (E) EDS spectra of whole yeast cell (gold spectra [front] and gold ellipse on STEM) and amorphous precipitates (red ellipse and red spectra [back]) depicting no presence of Gd inside cell walls and Gd-P co-localization.

No precipitates were observed in the larger areas of the epoxy (Supplementary Fig. S1), indicating that they must have originated close to the exterior of the cells. Cells were washed several times in buffer solution to remove excess media, so precipitates remaining in the sample must be generated in proximity to the cell exterior, or they would have been washed away during sample preparation.

While no facets were observed on the precipitates, selected area diffraction patterns were acquired in an effort to determine if there was a crystalline phase that could help identify the lanthanide compounds (Supplementary Fig. S2). A selected area diffraction pattern of the nanoprecipitates showed no defined rings consistent with polycrystalline material. Either the components were not well-ordered or the domain size was too small to cause diffraction, but the lack of evident crystallinity is consistent with the loose morphology. Nanobeam diffraction was also acquired with similar results. Repeated STEM imaging and EDS mapping with beam currents exceeding 100 pA was possible, and the precipitates did not exhibit beam sensitivity, indicating that they were strongly bound and stable compounds. Precipitate formation was not observed in cells not treated with lanthanides (Supplementary Fig. S3).

To further investigate the precipitates we identified several gadolinium compounds with a 1:1 ratio of metal to phosphorous through the Materials Project, primarily through the Materials Explorer tool.[34–36] $GdPO_4$ is insoluble in the biological pH range and has a relatively low predicted energy of formation, ΔH = −3.427 eV/atom, the most thermodynamically favorable Gd-P compound possible given EDS data and system constraints.[34,36–39] If toxicity is mediated through the lanthanide damaging the extracellular membrane and stripping out components of the phospholipid bilayer, $GdPO_4$ is an intriguing candidate. To explore this possibility further, we prepared a $GdPO_4$ TEM sample. $GdPO_4$ was formed in solution from a mixture of H_3PO_4 and $GdCl_3$ in aqueous media. The solution was cast onto TEM grids and a similar "seed-like" morphology was observed. EDS data from this synthesized $GdPO_4$ also indicated Gd:P ratio 1:1.5, which, though slightly higher than that measured in the yeast cell experiments, is plausible given that there may be excess phosphate on the grid (Supplementary Figs. S4 and S5). While we could not confirm that the nanoprecipitates present around the yeast cells were $GdPO_4$ through electron diffraction, the similar morphology shown by HAADF STEM and Gd:P ratio determined by EDS are evidence that this is a plausible possibility.

Saccharomyces cerevisiae strains with disruption of *sur 1* or both *csh1 and csg2* exhibit Ca^{2+} sensitivity by inhibiting proper ion transport mechanisms in the cell membrane, a mechanism which we previously thought lanthanides induce cytotoxicity as well.[26] When the gadolinium exposure was repeated with *csh1*, *csg2*, and *sur1* yeast mutants, we were surprised to observe EDS results consistent with the WT strain (Fig. 3). The mutant strains were more sensitive to lanthanides than the WT, however, and their growth was significantly more inhibited, particularly *sur1* (*vide infra*, Fig. 6).

To see if such growth inhibition was unique to gadolinium, we conducted additional experiments using europium and samarium, which are adjacent to gadolinium on the periodic table. Europium has been established to strongly affect cell membranes, producing pores and binding very tightly to phospholipids, while trivalent samarium has the same ionic radius as biologically relevant divalent calcium.[40] Treating WT yeast with samarium and europium resulted in metal-containing deposits outside the cells and near the cell surface with the same morphology as the gadolinium treated cells (Supplementary Figs. S6–S11). EDS was collected for various samarium and europium precipitates in the
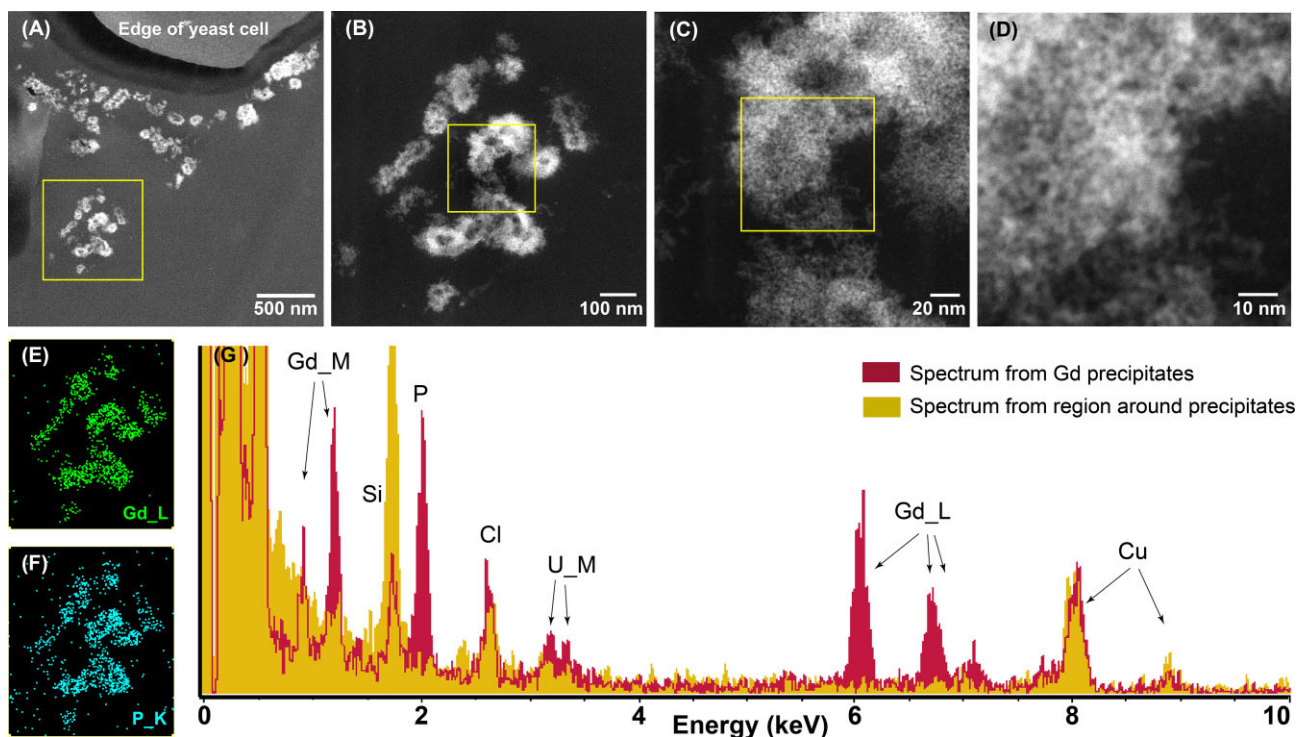
Fig. 2 Morphology of Gd precipitates. (A)–(D) HAADF-STEM images of nanoclusters of Gd co-located with P exhibited consistent morphology consisting of loose aggregates of ~1 nm non-crystalline particles presumed to be $GdPO_4$. (A) Precipitates are found adjacent to the yeast cell wall; (B) magnified image from yellow box in (A) shows aggregation with hollow center; (C) magnified image from yellow box in (B); (D) magnified image from yellow box in (C) shows individual clusters on the order of 1 nm; (E) and (F) EDS maps from Gd_L and P_K energy ranges, respectively, of same aggregation in (B); and (G) spectra from the EDS spectrum image. The red spectrum [back] is constructed from the pixels containing the bright aggregations while the gold spectrum [front] is from the area around the aggregation, which includes the microtome medium and background from the Cu grid and holder hardware. The gold spectrum does not contain the P and Gd signal present in the red spectrum. Quantification of the Gd:P ratio is ~1:1.
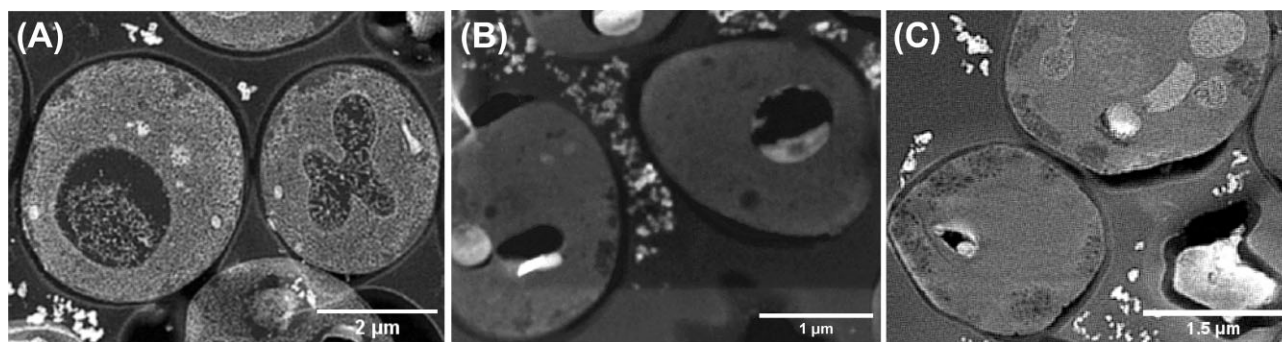

Fig. 3 Evidence that lanthanide precipitation outside of the cell is not dependent on some aspects of cell membrane integrity. (A) STEM of wild type strain treated with Gd. (B) sur1 mutant strain which exhibits impaired lipid phospholipid production treated with Gd. (C) sso2 mutant strain which exhibits Ln susceptibility as control, treated with Gd.

same manner as gadolinium-treated cells in a replica experiment, and like gadolinium, samarium, and europium precipitates were not found within the cells after exposure (Fig. 4). There is precedent for extracellular heavy metals accumulating on yeast cell walls, such as the spiky uranium formations observed by Strandberg *et al.*, and gold, platinum, silver, palladium, and rhodium deposits observed by others.[41–44]

EDS data showed that samarium, gadolinium, and europium precipitated outside of the yeast cells and provided further evidence of lanthanide-phosphorous co-localization (Fig. 4). This contrasts with the findings of Fingerhut *et al.*, who found no correlation between phosphorous and gadolinium localization in brain sections from GBCA-exposed patients.[44] We repeated the

lanthanide exposures and cell wash step with P-free HEPES to rule out the PBS wash buffer as the source of phosphorous and saw the same nanoprecipitation morphology and location outside of the cell wall. This suggests that the cells themselves are the source of phosphorous (Fig. 5), a finding supported by previous work by Pagnanelli *et al.*, which showed metal ions complexing with phosphate groups on the exterior of bacterial cells, which contain phosphate groups.[45] Since yeast cell walls are primarily composed of functionalized polysaccharides, it seems likely that the plasma membrane itself is the phosphate source. Additionally, research carried out by Goodman and Rothstein suggests that phosphate groups do not adhere to the cell wall, making cell wall bound phosphates as the primary source for precipitate formation
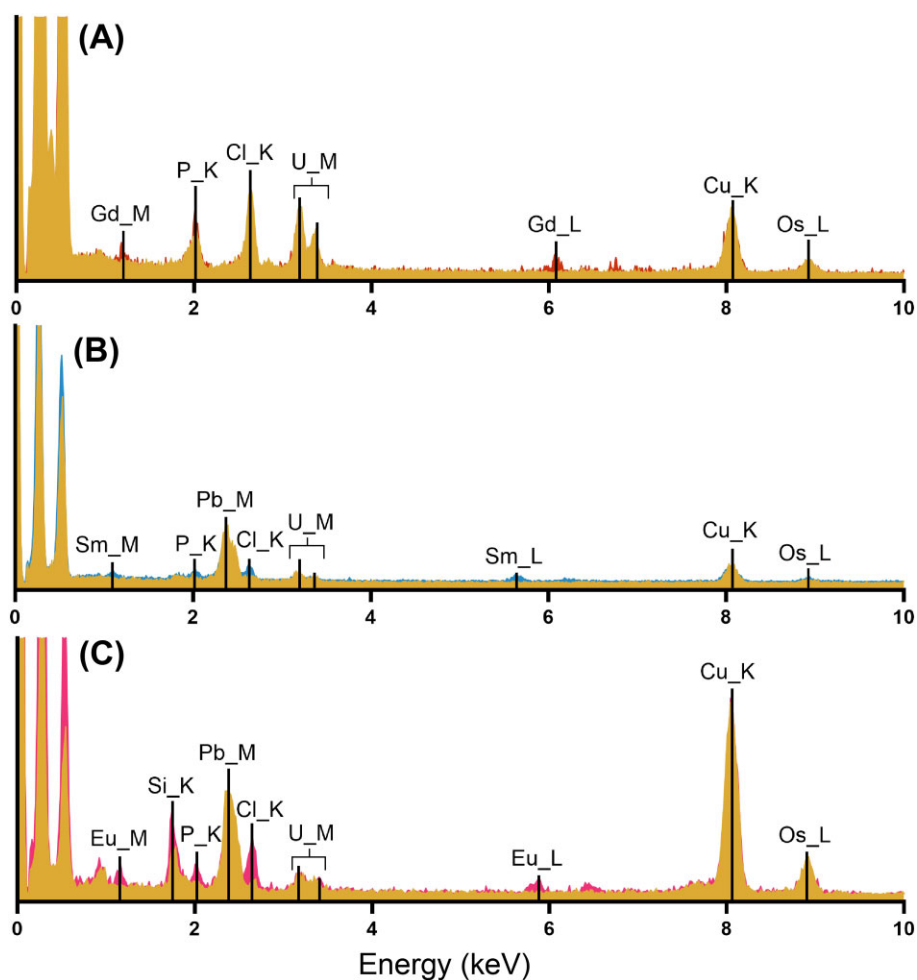
Fig. 4 Normalized spectra (to Cu peak) derived from EDS mapping of precipitates formed outside of the cell, with background (gold) [front] from the yeast cells themselves. (A) Gd treated cells (red) (B) Sm (blue) (C) Eu (pink) [back]. All precipitates still exhibit co-localization of Ln and P. Spectra are normalized to Cu_K peak.

unlikely.[46] Biosorption studies have shown that the different metals display different adsorption qualities, so we wanted to know if these three lanthanides would be significantly different from one another in this respect.

Growth data were collected using optical density measurements to assess lanthanide toxicity across WT and mutant strains. Among the strains with defective phosphosphingolipid production pathways (*sur1* and *csg2*), samarium was much more toxic to cells, followed by gadolinium, then europium, and the effect was reversed with the concurrent addition of Ca^{2+}. Following cell growth experiments for Sm, Eu, and Gd, the remaining lanthanides were investigated to identify trends in effects on cell growth following the addition of Ca^{2+} (Fig. 6). This experiment also has some precedent: work by Cui *et al.* reported that growth was inhibited by Ca^{2+} sensitive strains in the presence of high extracellular Ca^{2+}, but that growth was restored upon addition of small concentrations of Mg^{2+}.[47] Calcium is attracted to phospholipid head groups as well, similar to lanthanides, but does not disrupt membrane structure in a manner similar to lanthanides, by disrupting protein functions, except at high concentrations. Unexpectedly, combining two compounds known to diminish growth in these mutant strains resulted in improved cell growth across the series. A similar trend could be seen in the WT strain, although the differences between the metals were less striking. Taken together,

these observations show that plasma membrane composition and membrane transport capability affect the ability of lanthanide metals to affect yeast cells. From the data presented in Fig. 6, we may conclude that membrane composition is more important for resisting lanthanide adsorption than extracellular transport proteins, a finding that is consistent with previous work showing that yeast takes up heavy metals via passive, rather than active mechanisms.[48]

Conclusions

Our results support previous findings that gadolinium and other lanthanides can induce cellular toxicity without entering cells and suggest that these metals mediate their toxic effects extracellularly. Earlier studies have shown that lanthanides interact strongly with the negatively charged phospholipid head groups of lipid bilayers and that through this interaction, they cause deformation to the normal packing of phospholipid head groups, which in turn leads to disruption of membrane function.[12,49,50] Specifically, Cheng *et al.* describe lanthanide-induced pore formation in a lipid bilayer system.[16] From our observations in yeast, we propose the following mechanism for lanthanides: calcium competes with lanthanides to bind to the phospholipid head groups at the cytoplasmic membrane, and since neither metal
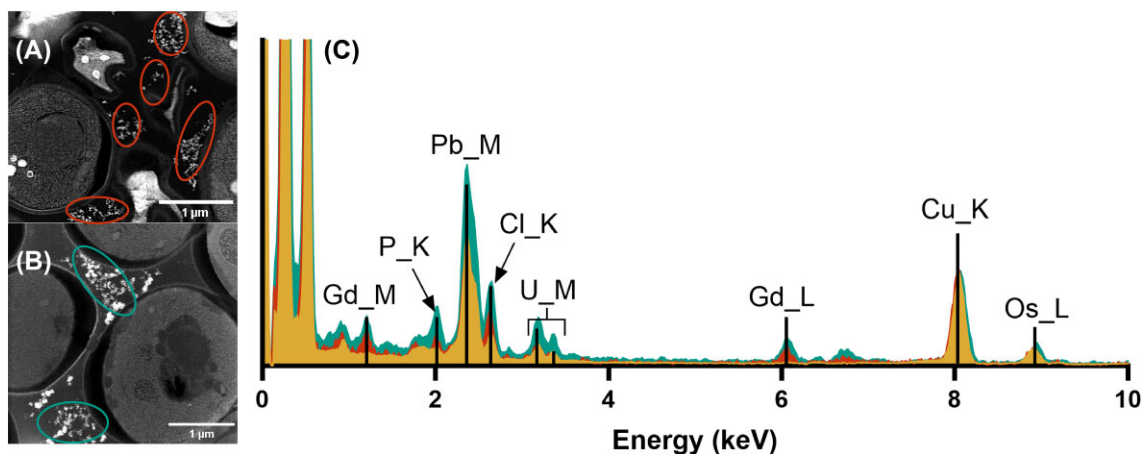
Fig. 5 STEM images and EDS spectra showing phosphorus and gadolinium co-localization outside of cells regardless of buffer solution used to prepare the cells. (A) Wild-type strain washed in HEPES, no P, precipitates outlined in red [middle]. (B) Wild-type strain washed in PBS, P containing, precipitates outlined in teal [back]. (C) Corresponding normalized spectra (to Cu peak) derived from EDS mapping; the gold spectra [front] is the cell area, in image (A), representative of background.
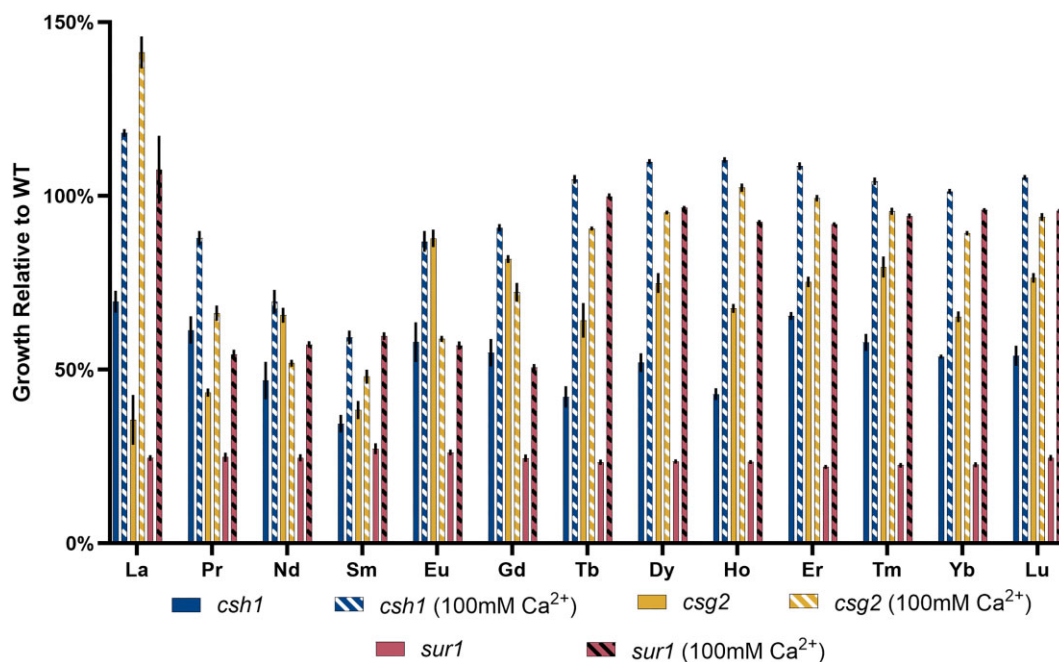

Fig. 6 Growth of yeast mutants relative to WT growth after 24 h of incubation time, as a function of lanthanide exposure and rescuing calcium concentration of selected mutant yeast strains, *csh1*, *csg2*, and *sur1* ($n = 4$). Bars in solid blue, yellow, and red shows the deleterious effect of lanthanides on yeast growth. Bars hashed blue, yellow, and red show treatment of lanthanide-exposed cells with calcium, which rescues them from the growth defect, even in calcium-sensitive strains. The experiments were performed in quadruplicates, error bars represent one standard deviation of the measurements. All cell viability Ca^{2+} treated viability measurements show significant difference to their respective controls with a *P*-value of <0.001 via multiple *t*-test (and non-parametric tests) analysis Supplementary Table S1.

can bind consistently, the membrane remains fluid and less distorted, rescuing the cells from the toxic effect. The excess calcium may then enter the cell and activate calcium-regulated cell cycle proteins, which leads to cellular proliferation. Surprisingly, the rescue effect was even observed in calcium-sensitive yeast strains. This is possibly explained by the fact that calcium regulates many intracellular processes—including the production of lipids for cell membranes—and a surfeit of calcium is highly disruptive to normal cell function. The competition between calcium and lanthanide metals appears to moderate deleterious effects of either substance.

The brain is a highly vascularized lipid-heavy organ and our results suggest that high lipid density is likely one reason that gadolinium (and presumably other lanthanides) accumulates there, having observed the metals clustered around the outside of yeast cell walls. Indeed, if lanthanides can mediate their toxicological effects at the level of the plasma membrane, we may speculate as to future research directions and potential risk factors for lanthanide sensitivity, and we plan to investigate nano-precipitation of $LnPO_4$ in mammalian cell lines. These findings suggest that patients with lipid disorders, or disorders involving components of the cellular membrane (transporters, receptors,

pores, channels) may be more vulnerable to lanthanide accumulation, and ultimately toxicity. It may therefore be worth investigating if there is a correlation between high body weight indices and patients who develop SAGE, including but not limited to NSF. Given that eicosanoids and other inflammatory compounds are derived from lipids, these pathways may present other avenues of study to explain why some patients develop SAGE and others do not.

Supplementary material

Supplementary data are available at *Metallomics* online.

Conflicts of interest

The authors declare no conflicts of interest.

References

1. V. Hatje, K.W. Bruland and A.R. Flegal, Increases in anthropogenic gadolinium anomalies and rare earth element concentrations in San Francisco bay over a 20 year record, *Environ. Sci. Technol.*, 2016, 50 (8), 4159–4168. https://doi.org/10.1021/acs.est.5b04322

2. K. Wang, R. Li, Y. Cheng and B. Zhu, Lanthanides—the future drugs?, *Coord. Chem. Rev.*, 1999, 192, 297–308. https://doi.org/10.1016/S0010-8545(99)00072-7

3. T. Grobner, Gadolinium—a specific trigger for the development of nephrogenic fibrosing dermopathy and nephrogenic systemic fibrosis?, *Nephrol. Dial. Transplant.*, 2006, 21 (4), 1104–1108. https://doi.org/10.1093/ndt/gfk062

4. P. Marckmann, L. Skov, K. Rossen, A. Dupont, M.B. Damholt, J.G. Heaf and H.S. Thomsen, Nephrogenic systemic fibrosis: suspected causative role of gadodiamide used for contrast-enhanced magnetic resonance imaging, *J. Am. Soc. Nephrol.*, 2006, 17 (9), 2359–2362. https://doi.org/10.1681/ASN.2006060601

5. T. Kanda, K. Ishii, H. Kawaguchi, K. Kitajima and D. Takenaka, High signal intensity in the dentate nucleus and globus pallidus on unenhanced T1-weighted MR images: relationship with increasing cumulative dose of a gadolinium-based contrast material, *Radiology*, 2014, 270 (3), 834–841. https://doi.org/10.1148/radiol.13131669

6. I.M. Braverman and S. Cowper, Nephrogenic systemic fibrosis, *F1000 Med. Rep.*, 2010, 2, 84. https://doi.org/10.3410/M2-84

7. A.S. Boyd, J.A. Zic and J.L. Abraham, Gadolinium deposition in nephrogenic fibrosing dermopathy, *J. Am. Acad. Dermatol.*, 2007, 56 (1), 27–30. https://doi.org/10.1016/j.jaad.2006.10.048

8. R.J. McDonald, J.C. Weinreb and M.S. Davenport, Symptoms associated with gadolinium exposure (SAGE): a suggested term, *Radiology*, 2022, 302 (2), 270–273. https://doi.org/10.1148/radiol.2021211349

9. W.A. High, J.F. Ranville, M. Brown, T. Punshon, A. Lanzirotti and B.P. Jackson, Gadolinium deposition in nephrogenic systemic fibrosis: an examination of tissue using synchrotron X-ray fluorescence spectroscopy, *J. Am. Acad. Dermatol.*, 2010, 62 (1), 38–44. https://doi.org/10.1016/j.jaad.2009.07.018

10. R.J. McDonald, J.S. McDonald, D.F. Kallmes, M.E. Jentoft, D.L. Murray, K.R. Thielen, E.E. Williamson and L.J. Eckel, Intracranial gadolinium deposition after contrast-enhanced MR imaging, *Radiology*, 2015, 275 (3), 772–782. https://doi.org/10.1148/radiol.15150025

11. S. Fingerhut, A.-C. Niehoff, M. Sperling, A. Jeibmann, W. Paulus, T. Niederstadt, T. Allkemper, W. Heindel, M. Holling and U. Karst, Spatially resolved quantification of gadolinium deposited in the brain of a patient treated with gadolinium-based contrast agents, *J. Trace Elem. Med. Biol.*, 2018, 45, 125–130. https://doi.org/10.1016/j.jtemb.2017.10.004

12. Y.A. Ermakov, K. Kamaraju, K. Sengupta and S. Sukharev, Gadolinium ions block mechanosensitive channels by altering the packing and lateral pressure of anionic lipids, *Biophys. J.*, 2010, 98 (6), 1018–1027. https://doi.org/10.1016/j.bpj.2009.11.044

13. R.S. Prosser, H. Bryant, R.G. Bryant and R.R. Vold, Lanthanide chelates as bilayer alignment tools in nmr studies of membrane-associated peptides, *J. Magn. Reson.*, 1999, 141 (2), 256–260. https://doi.org/10.1006/jmre.1999.1855

14. C. Ma and S.J. Opella, Lanthanide ions bind specifically to an added "EF-hand" and orient a membrane protein in micelles for solution NMR spectroscopy, *J. Magn. Reson.*, 2000, 146 (2), 381–384. https://doi.org/10.1006/jmre.2000.2172

15. A. Pałasz and P. Czekaj, Toxicological and cytophysiological aspects of lanthanides action, *Acta Biochim. Pol.*, 2000, 47 (4), 1107–1114. https://doi.org/10.18388/abp.2000_3963

16. Y. Cheng, M. Liu, R. Li, C. Wang, C. Bai and K. Wang, Gadolinium induces domain and pore formation of human erythrocyte membrane: an atomic force microscopic study, *Biochim. Biophys. Acta (BBA)—Biomembranes*, 1999, 1421 (2), 249–260. https://doi.org/10.1016/S0005-2736(99)00125-X

17. L. Gorniak, J. Bechwar, M. Westermann, F. Steiniger and C.E. Wegner, Different lanthanide elements induce strong gene expression changes in a lanthanide-accumulating methylotroph, *Microbiol. Spectr.*, 2023, 11 (6), e00867–e00823. https://doi.org/10.1128/spectrum.00867-23

18. N.M. Good, H.D. Lee, E.R. Hawker, M.Z. Su, A.A. Gilad and N.C. Martinez-Gomez, Hyperaccumulation of gadolinium by Methylorubrum extorquens AM1 reveals impacts of lanthanides on cellular processes beyond methylotrophy, *Front. Microbiol.*, 2022, 13, https://doi.org/10.3389/fmicb.2022.820327

19. P. Roszczenko-Jasińska, H.N. Vu, G.A. Subuyuj, R.V. Crisostomo, J. Cai, N.F. Lien, E.J. Clippard, E.M. Ayala, R.T. Ngo, F. Yarza, J.P. Wingett, C. Raghuraman, C.A. Hoeber, N.C. Martinez-Gomez and E. Skovran, Gene products and processes contributing

to lanthanide homeostasis and methanol metabolism in Methylorubrum extorquens AM1, *Sci. Rep.*, 2020, 10 (1), 12663. https://doi.org/10.1038/s41598-020-69401-4

20. C.-E. Wegner, M. Westermann, F. Steiniger, L. Gorniak, R. Budhraja, L. Adrian and K. Kusel, Extracellular and intracellular lanthanide accumulation in the methylotrophic Beijerinckiaceae bacterium RH AL1, *Appl. Environ. Microb.*, 2021, 87 (13), e03144–e03120.

21. S.N. Misra, M.A. Gagnani and R.S. Shukla, Biological and clinical aspects of lanthanide coordination compounds, *Bioinorg. Chem. Appl.*, 2004, 2 (3-4), 155–192. https://doi.org/10.1155/S1565363304000111

22. T.L. Fuller and R.G. Canada, Enhancement of cisplatin cytotoxicity by terbium in cisplatin-resistant MDA/CH human breast cancer cells, *Cancer Chemother. Pharmacol.*, 1999, 44 (3), 249–252. https://doi.org/10.1007/s002800050974

23. J.C. Parker and G.J. Barritt, Evidence that lanthanum ions stimulate calcium inflow to isolated hepatocytes, *Biochem. J.*, 1981, 200 (1), 109–114. https://doi.org/10.1042/bj2000109

24. R.M. Pallares, D. Faulkner, D.D. An, S. Hebert, A. Loguinov, M. Proctor, J.A. Villalobos, K.A. Bjornstad, C.J. Rosen, C. Vulpe and R.J. Abergel, Genome-wide toxicogenomic study of the lanthanides sheds light on the selective toxicity mechanisms associated with critical materials, *Proc. Natl. Acad. Sci. U.S.A.*, 2021, 118 (18), e2025952118. https://doi.org/10.1073/pnas.2025952118

25. T. Beeler, D. Bacikova, K. Gable, L. Hopkins, C. Johnson, H. Slife and T.M. Dunn, The *Saccharomyces cerevisiae* TSC10/YBR265w gene Encoding 3-ketosphinganine reductase is identified in a screen for temperature-sensitive suppressors of the Ca^{2+}-sensitive csg2Δ Mutant, *J. Biol. Chem.*, 1998, 273 (46), 30688–30694. https://doi.org/10.1074/jbc.273.46.30688

26. T.J. Beeler, D. Fu, J. Rivera, E. Monaghan, K. Gable and T.M. Dunn, SUR1 (CSG1 /BCL21), a gene necessary for growth of *Saccharomyces cerevisiae* in the presence of high Ca^{2+} concentrations at 37°C, is required for mannosylation of inositolphosphorylceramide, *Mol. Gen. Genet.*, 1997, 255 (6), 570–579. https://doi.org/10.1007/s004380050530

27. E.A. Winzeler, D.D. Shoemaker, A. Astromoff, H. Liang, K. Anderson, B. Andre, R. Bangham, R. Benito, J.D. Boeke, H. Bussey, A.M. Chu, C. Connelly, K. Davis, F. Dietrich, S. Whelen Dow, M. El Bakkoury, F. Foury, S.H. Friend, E. Gentalen, G. Giaever, J.H. Hegemann, T. Jones, M. Laub, H. Liao, N. Liebundguth, D.J. Lockhart, A. Lucau-Danila, M. Lussier, N. M'Rabet, P. Menard, M. Mittmann, C. Pai, C. Rebischung, J.L. Revuelta, L. Riles, C.J. Roberts, P. Ross-MacDonald, B. Scherens, M. Snyder, S. Sookhai-Mahadeo, R.K. Storms, S. Véronneau, M. Voet, G. Volckaert, T.R. Ward, R. Wysocki, G.S. Yen, K. Yu, K. Zimmermann, P. Philippsen, M. Johnston and R.W. Davis, Functional characterization of the S. cerevisiae genome by gene deletion and parallel analysis, *Science*, 1999, 285 (5429), 901–906. https://doi.org/10.1126/science.285.5429.901

28. R. M. Pallares, D. D. An, S. Hébert, D. Faulkner, A. Loguinov, M. Proctor, J.A. Villalobos, K.A. Bjornstad, C.J. Rosen, C. Vulpe and R.J. Abergel, Delineating toxicity mechanisms associated with MRI contrast enhancement through a multidimensional toxicogenomic profiling of gadolinium, *Mol. Omics*, 2022, 18 (3), 237–248. https://doi.org/10.1039/D1MO00267H

29. A. Espinel-Ingroff, D. Montero and E. Martin-Mazuelos, Long-term preservation of fungal isolates in commercially prepared cryogenic microbank vials, *J. Clin. Microbiol.*, 2004, 42 (3), 1257–1259.

30. K.l McDONALD and R.i. Webb, Freeze substitution in 3 hours or less, *J. Microscopy*, 2011, 243 (3), 227–233. https://doi.org/10.1111/j.1365-2818.2011.03526.x

31. M.S. Cyert and C.C. Philpott, Regulation of cation balance in *Saccharomyces cerevisiae*, *Genetics*, 2013, 193 (3), 677–713. https://doi.org/10.1534/genetics.112.147207

32. S. Ariponnammal, S. Shalini and S.N. Devi, Structural, surface morphological and low temperature studies on gadolinium trichloride ($GdCl_3$), *Mater. Today Proc.*, 2021, 35, 39–43.

33. R. Wright, Transmission electron microscopy of yeast, *Microsc. Res. Tech.*, 2000, 51 (6), 496–510. https://doi.org/10.1002/1097-0029(20001215)51:6<496::AID-JEMT2>3.0.CO;2-9

34. A. Jain, S.P. Ong, G. Hautier, W. Chen, W.D. Richards, S. Dacek, S. Cholia, D. Gunter, D. Skinner, G. Ceder and K.A. Persson, Commentary: the Materials Project: a materials genome approach to accelerating materials innovation, *APL Mater.*, 2013, 1 (1), 011002. https://doi.org/10.1063/1.4812323

35. M. Aykol, S.S. Dwaraknath, W. Sun and K.A. Persson, Thermodynamic limit for synthesis of metastable inorganic materials, *Sci. Adv.*, 2018, 4 (4), eaaq0148. https://doi.org/10.1126/sciadv.aaq0148

36. A.K. Singh, L. Zhou, A. Shinde, S.K. Suram, J.H. Montoya, D. Winston, J.M. Gregoire and K.A. Persson, Electrochemical stability of metastable materials, *Chem. Mater.*, 2017, 29 (23), 10159–10167. https://doi.org/10.1021/acs.chemmater.7b03980

37. R. Tran, Z. Xu, B. Radhakrishnan, D. Winston, W. Sun, K.A. Persson and S.P. Ong, Surface energies of elemental crystals, *Sci. Data*, 2016, 3 (1), 160080. https://doi.org/10.1038/sdata.2016.80

38. M. de Jong, W. Chen, T. Angsten, A. Jain, R. Notestine, A. Gamst, M. Sluiter, C.K. Ande, S. van der Zwaag, J.J. Plata, C. Toher, S. Curtarolo, G. Ceder, K.A. Persson and M. Asta, Charting the complete elastic properties of inorganic crystalline compounds, *Sci. Data*, 2015, 2 (1), 150009. https://doi.org/10.1038/sdata.2015.9

39. K. Latimer, S. Dwaraknath, K. Mathew, D. Winston and K.A. Persson, Evaluation of thermodynamic equations of state across chemistry and structure in the materials project, *NPJ Comput. Mater.*, 2018, 4 (1), 1–7. https://doi.org/10.1038/s41524-018-0091-x

40. J.C. Slater, Atomic radii in crystals, *J. Chem. Phys.*, 1964, 41 (10), 3199–3204. https://doi.org/10.1063/1.1725697

41. G.W. Strandberg, S.E. Shumate and J.R. Parrott, Microbial cells as biosorbents for heavy metals: accumulation of uranium by *Saccharomyces cerevisiae* and *Pseudomonas aeruginosa*, *Appl. Environ. Microb.*, 1981, 41 (1), 237–245. https://doi.org/10.1128/aem.41.1.237-245.1981

42. D.D. Xie, Y.Y. Liu and C.L. Wu, Studies of Properties on the immobilized *Saccharomyces cerevisiae* waste biomass adsorbing Pt^{4+}, *J. Xiamen Univ.*, 2003, 42, 800–804.

43. D.D. Xie, Y.Y. Liu and C.L. Wu, Studies on biosorption of Pd^{2+} by the immobilized *Saccharomyces cerevisiae* waste biomass, *Microbiology*, 2003, 30, 29–34.

44. S. Fingerhut, M. Sperling, M. Holling, T. Niederstadt, T. Allkemper, A. Radbruch, W. Heindel, W. Paulus, A. Jeibmann and U. Karst, Gadolinium-based contrast agents induce gadolinium deposits in cerebral vessel walls, while the neuropil is not affected: an autopsy study, *Acta Neuropathol.*, 2018, 136 (1), 127–138. https://doi.org/10.1007/s00401-018-1857-4

45. F. Pagnanelli, A. Esposito and F. Vegliò, Multi-metallic modelling for biosorption of binary systems, *Water Res.*, 2002, 36 (16), 4095–4105. https://doi.org/10.1016/S0043-1354(02)00112-4

46. J. Goodman and A. Rothstein, The active transport of phosphate into the yeast cell, *J. Gen. Physiol.*, 1957, 40 (6), 915–923. https://doi.org/10.1085/jgp.40.6.915

47. J. Cui, J.A. Kaandorp, O.O. Ositelu, V. Beaudry, A. Knight, Y.F. Nanfack and K.W. Cunningham, Simulating calcium influx and free calcium concentrations in yeast, *Cell Calcium*, 2009, 45 (2), 123–132. https://doi.org/10.1016/j.ceca.2008.07.005

48. J. Wang and C. Chen, Biosorption of heavy metals by Saccharomyces cerevisiae: a review, *Biotechnol. Adv.*, 2006, 24 (5), 427–451. https://doi.org/10.1016/j.biotechadv.2006.03.001

49. Y.A. Ermakov, A.Z. Averbakh, A.I. Yusipovich and S. Sukharev, Dipole potentials indicate restructuring of the membrane interface induced by gadolinium and beryllium ions, *Biophys. J.*, 2001, 80 (4), 1851–1862. https://doi.org/10.1016/S0006-3495(01)76155-3

50. M.-P. Nieh, C.J. Glinka, S. Krueger, R.S. Prosser and J. Katsaras, SANS study on the effect of lanthanide ions and charged lipids on the morphology of phospholipid mixtures, *Biophys. J.*, 2002, 82 (5), 2487–2498. https://doi.org/10.1016/S0006-3495(02)75591-4